Available online at www.sciencedirect.com
ScienceDirect
Trans. Nonferrous Met. Soc. China 32(2022) 2852−2865
Transactions of Nonferrous Metals Society of China
www.tnmsc.cn

Solid solution strengthening and damping capacity of Mg−Ga binary alloys

Wen-sen HUANG[1,2], Ji-hua CHEN[1,2], Hong-ge YAN[1,2], Qiang LI[3], Wei-jun XIA[1,2], Bin SU[1,2], Wei-jun ZHU[1]

1. School of Materials Science and Engineering, Hunan University, Changsha 410082, China;
2. Hunan Provincial Key Laboratory of Spray Deposition Technology & Application, Hunan University, Changsha 410082, China;
3. Beijing Institute of Space Long March Vehicle, Beijing 100076, China

Received 26 September 2021; accepted 14 March 2022

Abstract: The mechanical behaviors and damping capacities of the binary Mg−Ga alloys with the Ga content ranging from 1 to 5 wt.% were investigated by means of optical microscope (OM), scanning electron microscope (SEM), X-ray diffraction (XRD), hardness test, tensile test and dynamic mechanical analyzer (DMA). The hardness ($HV_{0.5}$) increases with the increase of Ga content, which can be described as $HV_{0.5}=41.61+10.35c$, and the solid solution strengthening effect $\Delta\sigma_s$ of the alloy has a linear relationship with c^n, where c is the molar fraction of solute atoms and n=1/2 or 2/3. Ga exhibits a stronger solid solution strengthening effect than Al, Zn or Sn due to the large atomic radius difference and the modulus mismatch between Ga and Mg atoms. The addition of Ga makes the Mg−Ga alloys have better damping capacity, and this phenomenon can be explained by the Granato−Lücke dislocation model. The lattice distortion and the modulus mismatch generated because of the addition of Ga increase the resistance to motion of the dislocation in the process of swinging or moving, and thus the better damping capacity is acquired.
Key words: Mg−Ga alloys; solid solution strengthening; damping capacity; Granato−Lücke model

1 Introduction

In recent years, the Mg−Ga alloys have attracted more and more attention [1,2]. Some studies have shown that the Mg−Ga alloys have a great potential to become a new type of magnesium alloys with excellent comprehensive properties. Mg−Ga alloys have a great potential in the application of biological materials due to outstanding corrosion resistance, good biocompatibility and lower biological toxicity [3−6]. LIU et al [7] reported that the Mg−Ga alloys had age hardening characteristics and the strength of Mg−Ga alloys could be improved by aging treatment. KHOKHLOVA and KHOKHLOV [8] simulated the three-dimensional visible arrangement of atoms in the Mg−Ga alloys system, and proposed that there was a unique arrangement of atoms in the Mg−Ga alloys. WU et al [9] reported that the reversible hydrogen storage capacity of Mg−Ga alloys was 5.7 wt.% H_2, and concluded that Mg−Ga alloys have better hydrogen storage properties. The Ga element could promote dynamic recrystallization and weaken the basal texture of wrought Mg−Ga alloys, and the as-rolled Mg−Ga sheets had excellent comprehensive mechanical properties [10,11]. There were also a small number of investigations on the solid solution strengthening effect of Ga element. KAUBÁSEK et al [3,4] discovered that the

Corresponding author: Ji-hua CHEN, Tel: +86-731-88823554, E-mail: jihuachen2005@163.com;
Hong-ge YAN, E-mail: yanhg68@163.com
DOI: 10.1016/S1003-6326(22)65988-0
1003-6326/© 2022 The Nonferrous Metals Society of China. Published by Elsevier Ltd & Science Press

Ga element had a certain strengthening effect on Mg alloys and the strengthening effect of Ga was stronger than that of Sn. MOHEDANO et al [5] displayed that the Mg−Ga alloys exhibit higher hardness with the increase in Ga content. Similar to Al, Zn, Sn, Y, Gd and Cd, Ga also had high solid solubility in Mg [12]. So far, the solid solution strengthening effect of the binary alloys, such as Mg−Al [13], Mg−Zn [14], Mg−Sn [15], Mg−Y [16], Mg−Gd [17] and Mg−Cd [18], has been expensively studied, but that of the binary Mg−Ga alloys has not been systematically studied yet. Therefore, the exploration of solid solution strengthening of the Mg−Ga alloy is of great significance for the development of the Mg−Ga alloys.

Up to now, there have been a lot of studies on the factors that influenced the damping capacity of magnesium alloys, including grain size [19], second phase [20−23], alloying type [24,25], and deformation method [26,27]. These studies were analyzed on the basis of the Granato−Lücke (G−L) model proposed by GRANATO and LÜCKE [28,29]. The energy-dissipation source, which was generated when dislocation was cutting second phase particles, could improve the damping capacity of magnesium alloy [30]. In addition, the interaction between the dislocation and the stacking fault could also improve the damping capacity in the magnesium alloys [31] and Al−Mg alloys [32]. There is no doubt that when the alloying element is added to magnesium alloys, these atoms will inevitably interact with dislocations, and this interaction will affect the damping capacities of magnesium alloys. Although a large number of studies have been conducted on the damping capacities of magnesium alloys [19−31], there are few studies on the influence of solute atoms on the damping capacities from the perspective of the motion of dislocations. Although the damping capacity of Mg−1at.%Ga alloy can be seen in the reference [24], there are few systematic studies on the influence of Ga content on the damping capacity of Mg−Ga alloys.

In this work, the solution strengthening effects of the Mg−Ga alloy with different Ga contents are studied. It is found that the Ga element has a strong strengthening effect on magnesium alloys in comparison with the other binary magnesium alloys. Moreover, the damping capacity of the Mg−Ga alloys is also deeply analyzed and discussed.

2 Experimental

Pure Mg with the purity of 99.9% and pure Ga with the purity of 99.99% were used as the raw materials to prepare the binary Mg−Ga alloy ingots involved in the present study. The detailed preparation process of the ingots could be found in the reference [10]. Four Mg−Ga alloys (with the nominal Ga content of 1, 2, 3 and 5 wt.%) were prepared and labeled as Mg−1Ga, Mg−2Ga, Mg−3Ga and Mg−5Ga, respectively. The Mg−Ga ingots experienced a solid solution treatment at the temperature of 375 °C for 10−12 h. For comparison, a new group of the solid solution treated Mg−1Ga, Mg−3Ga and Mg−5Ga alloys are once again selected, they are kept at 460 °C for 1, 6 and 8 h, respectively, and defined as Mg−1Ga#, Mg−3Ga# and Mg−5Ga#, respectively. Finally, all the Mg−Ga ingots were quenched into water. The microstructures of Mg−Ga alloys were examined by a LeitzMM-6 optical microscope (OM) after Mg−Ga alloys were etched in a solution of 0.3 g picric acid, 1 mL acetic acid, 1.5 mL water and 10 mL alcohol. The phase constitutions were analyzed by a D5000 X-ray diffraction (XRD) instrument with Cu K_α at a scanning rate of 6 (°)/min. The FEI Quanta 200 scanning electron microscope (SEM) equipped with EDAX genesis xm-2 energy spectrometer (EDS) was used to analyze the microstructures of the solid solution treated alloys. The average grain size was measured by the intercept method on the basis of the optical images. The hardness test was performed on a Vickers hardness tester with a load of 0.98 N and a retention time of 15 s. Each sample had no less than 9 indentations. Tensile samples were cut from the Mg−Ga alloys which experienced solution treatment and were machined into 55 mm × 4 mm × 2 mm in gauge size. Tensile test was conducted on the Instron 3369 instrument with the initial tensile strain rate of 1.1×10^{-3} s^{-1}, and at least three tests were carried out under all the test conditions in order to improve the reliability of experimental data.

Four kinds of measurements are usually applied to expressing the damping capacities of materials as follows [33,34]: (1) The logarithmic decrement (δ) method expressed by $\delta=\ln(A_i/A_{i+1})$ from the amplitude of vibration A_i at the ith

vibration cycle and A_{i+1} at the (i+1)th vibration cycle; (2) The specific damping capacity (SDC, C_{SD}) method expressed by $C_{SD}=\Delta W/W$ from the dissipated energy ΔW of any vibration cycle divided by system energy W of the vibration cycle; (3) The inverse quality factor Q^{-1} method expressed by $Q^{-1}=\Delta f_r/f_r$, where f_r is the resonance frequency (Hz), Δf_r is the half-power bandwidth at the resonance peak of f_r (Hz); (4) The method of tangent phase angle φ expressed by tan φ from measured stress σ and strain ε. It should be emphasized that the inverse quality factor Q^{-1} is equal to the tangent phase angle φ, i.e., $Q^{-1}=\tan\varphi$. The relationships among aforementioned four parameters for describing damping properties can be correlated under the condition of small strain as follows [34]:

$$\delta/\pi=C_{SD}/(2\pi)=Q^{-1}=\tan\varphi \quad (1)$$

The damping properties of prepared samples of as-solutionized binary Mg−Ga alloys were measured by the method of tangent phase angle φ, i.e., tan φ, through a dynamic mechanical analyzer (DMA) produced by TA Instruments in a type of Q800 (Q800−DMA) in the single cantilever vibration mode with the sample sizes of 30 mm × 3 mm × 1 mm at room temperature, and the strain amplitude (ε) ranged from 0.001% to 1% and the vibration frequency was set at 1 Hz. The temperature-dependent damping testing was conducted from room temperature to 400 °C at a heating rate of 5 °C/min, with the strain amplitude of 0.004% and the vibration frequency of 1 Hz.

3 Results

3.1 Microstructures

The as-cast and as-solutionized microstructures of the Mg−Ga alloys with different Ga contents are presented in Fig. 1. As shown in Figs. 1(a−d), there are second phases in as-cast Mg−Ga alloys, which are distributed along the grain boundary, and the volume fraction of these second phases increases with the increase of Ga content. Combined with the XRD results in Fig. 2(a), it is concluded that the second phase is the Mg_5Ga_2 phase. The OM images of the solid solution treated alloys are displayed in Figs. 1(e−h). The second phase in the as-cast alloy disappears after solution treatment. At the same time, according to the XRD results in Fig. 2(a), the alloys after solution treatment are the single-phase α-Mg. It can be seen from Fig. 2(b) that the lattice distortion caused by the addition of Ga atoms makes the Mg peak shift to a high angle. The EDS analyses of randomly selected regions in solid solution treated alloys are manifested in Fig. 3. As seen from Fig. 3, the second phase particles are dissolved in the matrix and the Ga element is uniformly distributed in the matrix. The molar fraction of the four alloys shown in Table 1 are relatively close to 1 wt.% (0.35 at.%), 2 wt.% (0.71 at.%), 3 wt.% (1.06 at.%), 5 wt.% (1.80 at.%). With the increasing Ga content, the grain size of the alloy is refined obviously and the change of grain size with the Ga content is summarized in Table 1. The average grain size of as-cast alloy is refined from (78±20) μm of Mg−1Ga to (47±13) μm of Mg−5Ga, and the grain size is refined by about 40%. The average grain sizes of the four solid solution treated Mg−Ga alloys are (91±30), (74±27), (67±18) and (58±18) μm, respectively.

3.2 Ga content dependence of solid solution strengthening

The mechanical properties of solid solution treated Mg−Ga alloys are displayed in Fig. 4. As shown in Fig. 4(a), with the increase of Ga content, the hardness of the alloy increases monotonously, from HV 46 of Mg−1Ga to HV 61 of Mg−5Ga, with an increase of 33%. The engineering stress−strain curves of the solid solution treated Mg−Ga alloys are presented in Fig. 4(b). The change of tensile properties with the Ga content is shown in Fig. 4(c). The yield strength, tensile strength and elongation of the alloy increase with the increasing Ga content. Two strengthening mechanisms, i.e. solid solution strengthening and fine grain strengthening, play roles in the single-phase Mg−Ga alloys, which will be carefully discussed in the following.

3.3 Damping properties of Mg−Ga alloys

The strain-amplitude-dependent damping properties of the solid solution treated Mg−Ga alloys tested at 1 Hz and ambient temperature are presented in Fig. 5. All the strain-amplitude-dependent damping curves can be divided into two parts. One is the part in which the damping is independent or weakly related to the strain amplitude, and the other is the part in which the

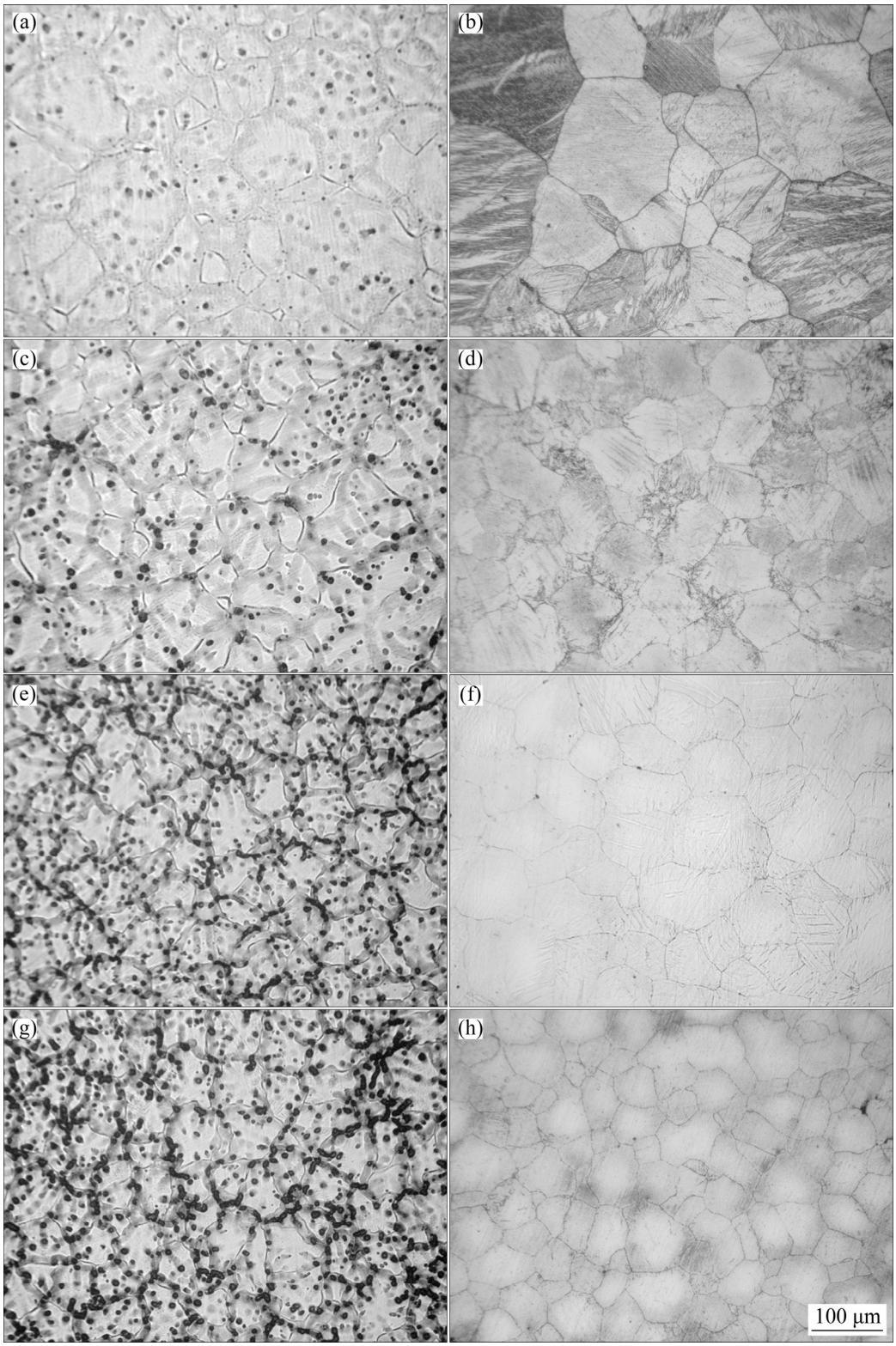

Fig. 1 Microstructures of as-cast (a, c, e, g) and as-solutionized (b, d, f, h) Mg−Ga alloys: (a, b) Mg−1Ga; (c, d) Mg−2Ga; (e, f) Mg−3Ga; (g, h) Mg−5Ga

damping capacity increases sharply with the increase of strain amplitude. The strain amplitude corresponding to the inflection point of these two parts is the first critical strain amplitude (ε_{cr1}) [33,35]. The ε_{cr1} values of Mg−1Ga, Mg−2Ga, Mg−3Ga, Mg−5Ga alloys are 0.0159%, 0.0229%, 0.0463%, and 0.0544%, respectively. When the strain amplitude is greater than ε_{cr1}, the damping

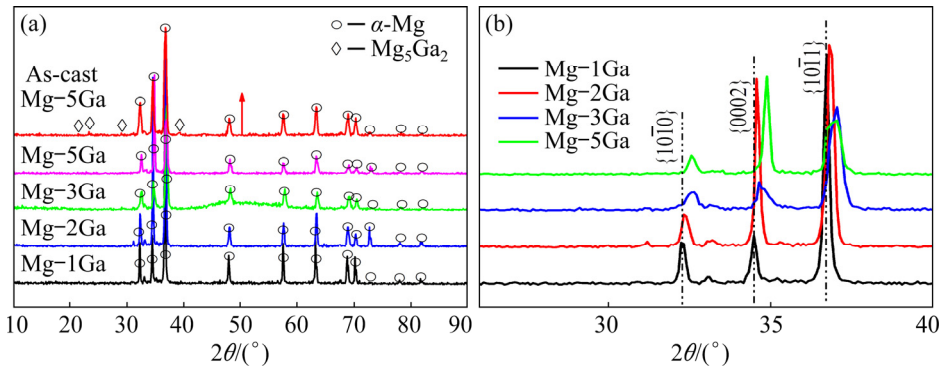

Fig. 2 XRD patterns of as-cast Mg−5Ga and as-solutionized Mg−Ga alloys (a), and $\{10\bar{1}0\}$, {0002} and $\{10\bar{1}1\}$ peaks of as-solutionized Mg−Ga alloys (b)

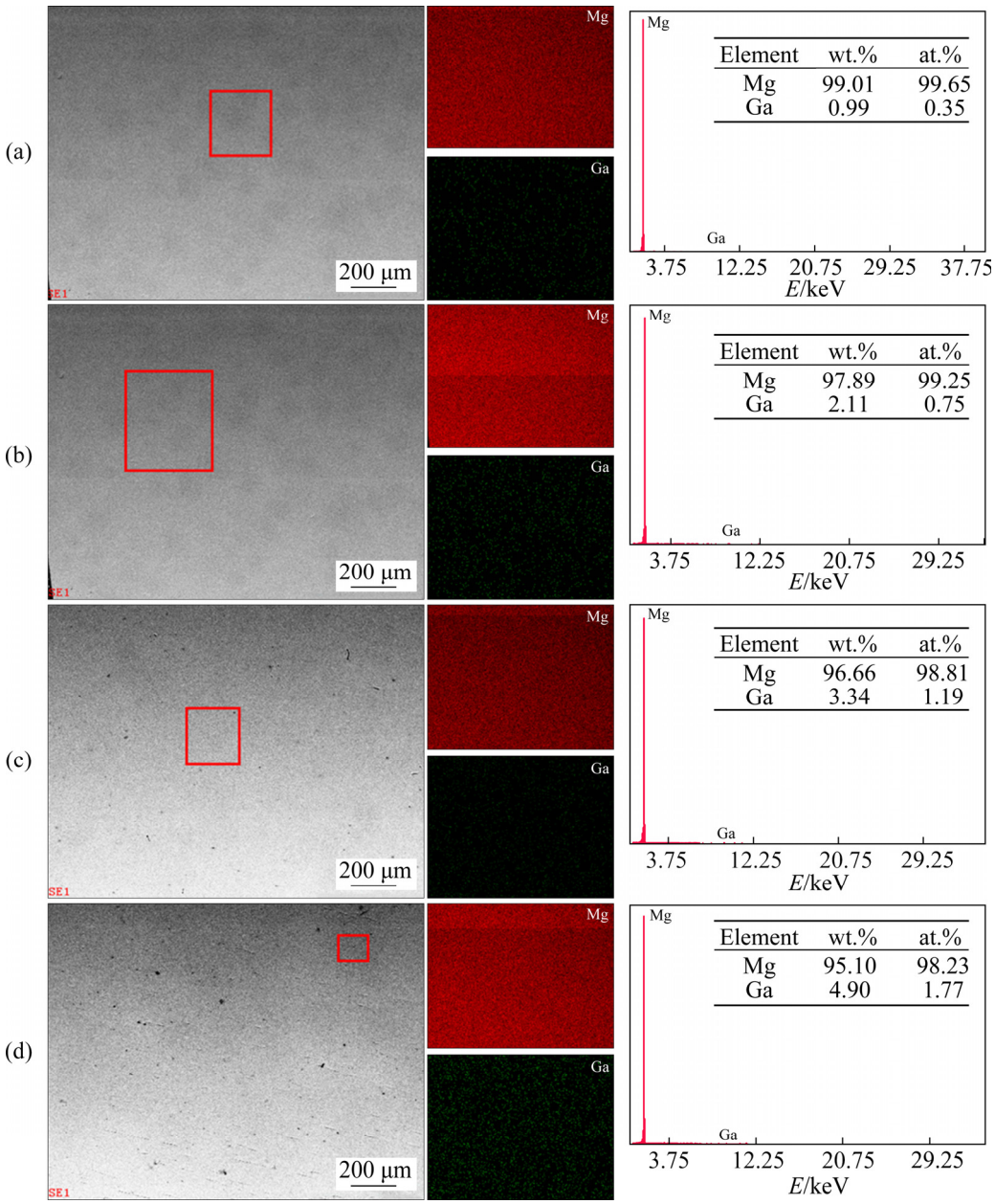

Fig. 3 EDS mappings of randomly selected regions in solid solution treated Mg−Ga alloys: (a) Mg−1Ga; (b) Mg−2Ga; (c) Mg−3Ga; (d) Mg−5Ga

Table 1 Chemical compositions and average grain sizes of Mg−Ga alloys

Alloy	Nominal content/ wt.% (at.%)	Analyzed content/ wt.% (at.%)	Average grain size/μm	
			As-cast	As-solutionized
Mg−1Ga	1 (0.35)	0.99 (0.35)	78±20	91±30
Mg−2Ga	2 (0.71)	2.11 (0.75)	58±16	74±27
Mg−3Ga	3 (1.06)	3.34 (1.19)	54±19	67±18
Mg−5Ga	5 (1.80)	4.90 (1.77)	47±13	58±18

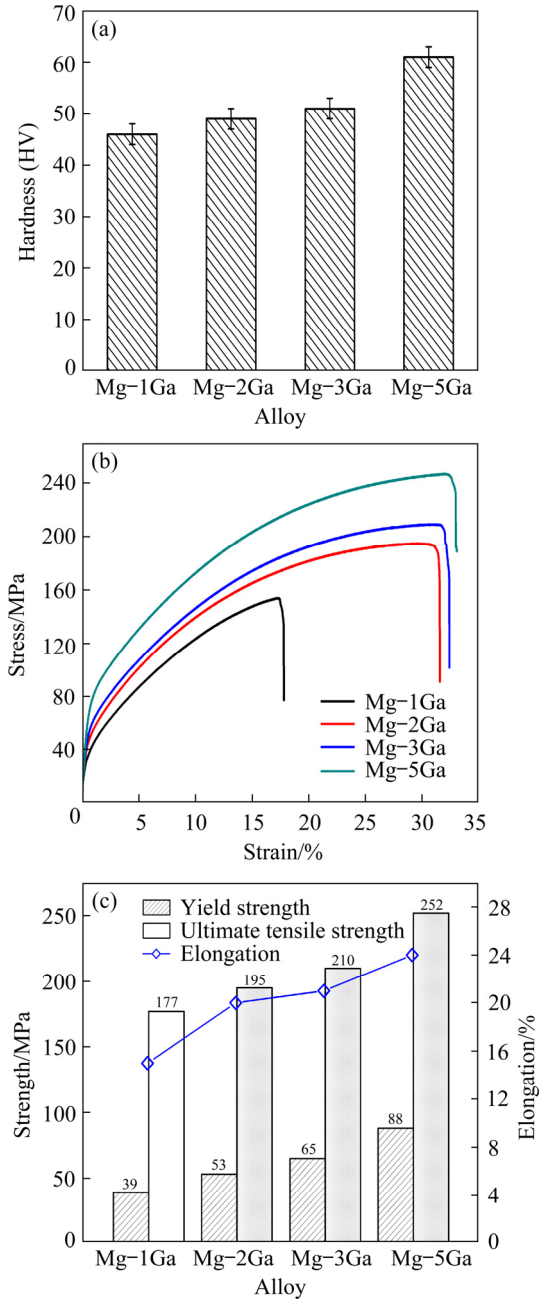

Fig. 4 Mechanical properties of solid solution treated Mg−Ga alloys at room temperature: (a) Hardness change; (b) Engineering stress−strain curves; (c) Tensile properties

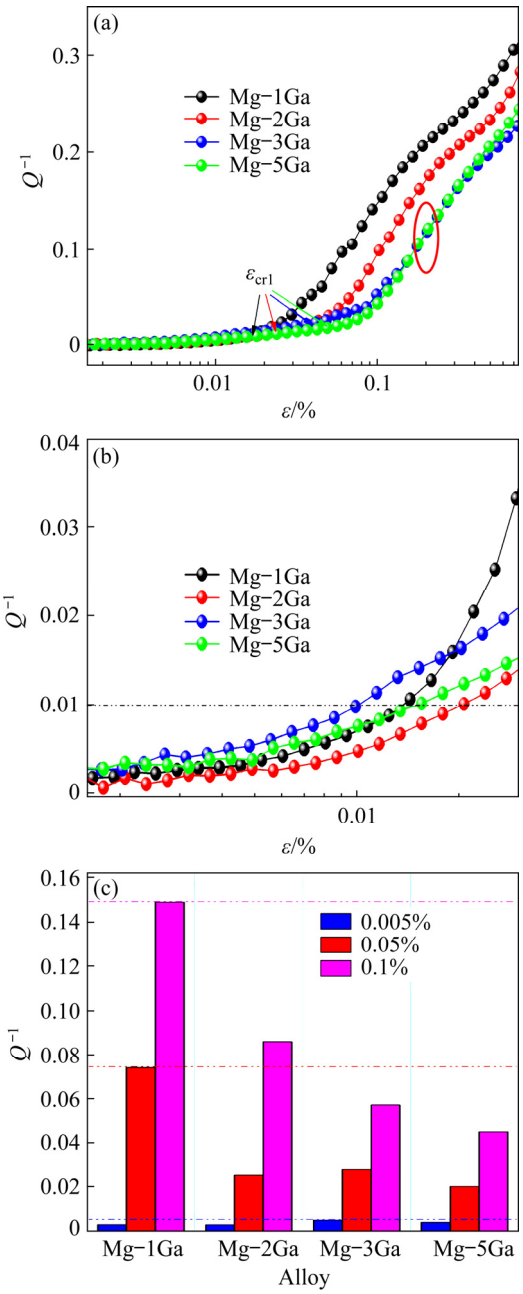

Fig. 5 Strain-amplitude-dependent damping properties of solid solutionized Mg−Ga alloys: (a) Damping strain amplitude curves; (b) Magnification curve under low strain amplitude; (c) Comparison of damping capacity under different strain amplitudes

capacity increases sharply with the higher strain amplitude and the alloy with the higher Ga content has a higher growth rate. The Mg−5Ga alloy has the highest ε_{cr1}, and when the strain amplitude is about 0.15%, its damping capacity is similar to that of Mg−3Ga (circled by red in Fig. 5(a)). With the continuing increase of the strain amplitude, the Mg−5Ga alloy exhibits higher damping capacity than the Mg−3Ga alloy. Figure 5(b) shows the

enlarged diagram of the damping capacity at low strain amplitudes in Fig. 5(a). The damping capacities of Mg−1Ga, Mg−2Ga, Mg−3Ga and Mg−5Ga reach the high damping level of 0.01 [36] at the strain amplitudes of 0.014%, 0.02%, 0.01%, and 0.015%, respectively, and all the strain amplitudes are less than the corresponding ε_{cr1}. Therefore, the Mg−Ga alloys reach a high damping level before the ε_{cr1}, which means that the external energy applied to the alloys can be dissipated before the dislocations break away the weak pinning point, which is of importance to engineering application. Figure 5(c) shows that the damping capacities of Mg−3Ga and Mg−5Ga alloys under the low strain amplitude are higher than those of Mg−1Ga and Mg−2Ga alloys, which is contrary to the trend in the references [37,38]. The possible reasons for this phenomenon will be carefully discussed later. The damping capacities of the Mg−Ga alloys decrease with the higher Ga content under the high strain amplitude, and that of Mg−1Ga alloy reaches 0.149 with the strain amplitude of 0.1%.

In order to control the single variable, Mg−Ga alloys with the same grain size are employed for further study. After isothermal heat treatment at 460 °C, the grain sizes of the three alloys are almost the same (about 120 μm, shown in Figs. 6(a−c)). Then the damping performance is tested, and the test results are shown in Fig. 6(d). It can be found that the changing trend of Fig. 6(d) is the same as that of Fig. 5(a). When the strain amplitude is greater than ε_{cr1}, the damping capacity increases rapidly with the increase of strain amplitude for the three alloys. It is worth noting that the Mg−5Ga# alloy with high Ga content has the fastest growth trend, which means that it exhibits higher damping capacity than those of the Mg−1Ga# and Mg−3Ga# alloys at high strain amplitude (see the circle in Fig. 6(d)).

The temperature damping test is adopted and the result is illustrated in Fig. 7. The strain amplitude is 0.004%, the test frequency is 1 Hz and the test temperature range is 30−400 °C. Compared with the ε_{cr1} data mentioned earlier, under such a strain amplitude, the dislocations in all the alloys don't break away from the weak pinning point, and the dislocations only swing between the weak pinning points. But at the same time, the increase in temperature can increase the motion of dislocations. As illustrated in Fig. 7, the damping capacity of Mg−5Ga is the best in the whole test temperature range.

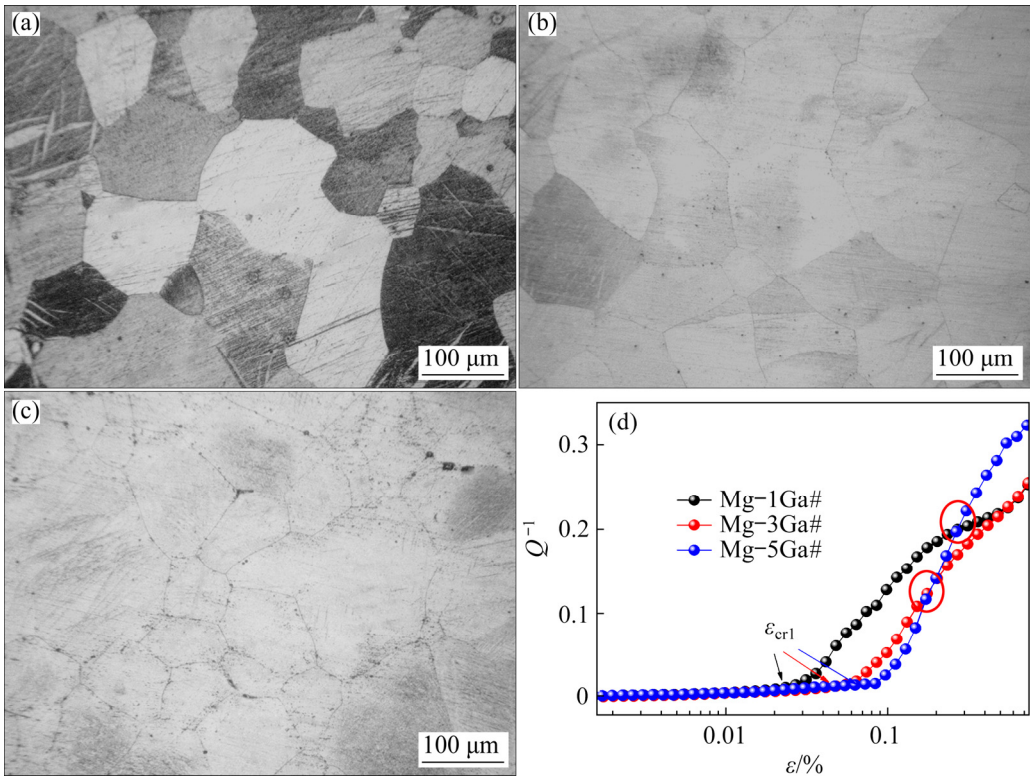

Fig. 6 Optical images of alloys after grain growth: (a) Mg−1Ga#; (b) Mg−3Ga#; (c) Mg−5Ga#; (d) Strain-amplitude-dependent damping properties of Mg−Ga alloys with same grain size

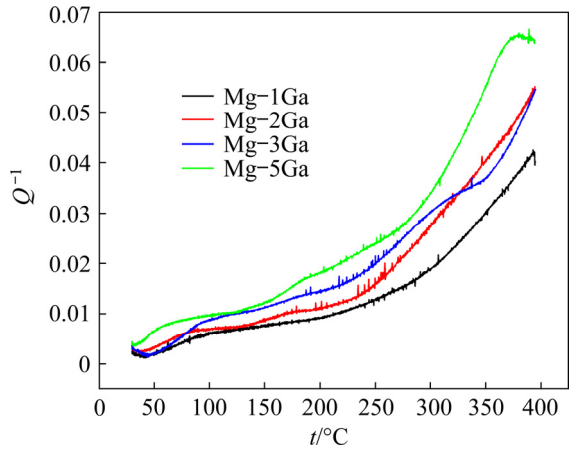

Fig. 7 Damping capacity versus temperature curves of Mg−Ga alloys

4 Discussion

4.1 Solid solution strengthening

As shown in Fig. 8, the hardness of the alloy increases monotonously with the increase of Ga content. The similar data of Mg−Al [13], Mg−Zn [14], Mg−Sn [15], Mg−Y [16], and Mg−Gd [17] alloys are also included in Fig. 8 for comparison. These data show the same trend except for the slope. The best linear fitting curve shows that the hardness ($HV_{0.5}$) of the alloy is related to the Ga content and this linear relationship can be expressed by

$$HV_{0.5}=41.61+10.35c \quad (R^2=0.957) \tag{2}$$

where $HV_{0.5}$ is the Vickers hardness in kg/mm^2, c is the Ga content in at.%, and R^2 is the correction coefficient. The hardness of the alloy increases almost linearly with the Ga content, about

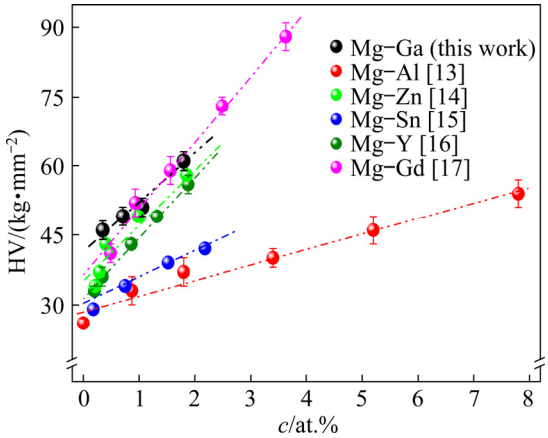

Fig. 8 Effect of Ga content on hardness of Mg−Ga alloys with Mg−Al, Mg−Zn, Mg−Sn, Mg−Y and Mg−Gd alloys for comparison

10.35 kg/(mm^2·at.%) Ga, which is higher than the values of Mg−Al alloys [13] (≈3 kg/(mm^2·at.%) Al), Mg−Zn alloys [14] (≈9 kg/(mm^2·at.%) Zn) and Mg−Sn alloys [15] (≈6.88 kg/(mm^2·at.%) Sn), but lower than those of Mg−Y alloys [16] (≈13.23 kg/(mm^2·at.%) Y) and Mg−Gd alloys [17] (≈14 kg/(mm^2·at.%) Gd). The hardening effect of Ga is only weaker than that of rare earth (Y and Gd).

The strengthening effect caused by grain refinement can be explained quantitatively by the Hall−Petch equation [39]:

$$\Delta\sigma_g=\sigma_0+kd^{-1/2} \tag{3}$$

where σ_0 is 11 MPa·μm$^{1/2}$ for pure magnesium [14,15,17], k is a constant determined by polycrystalline materials, and d is the grain size. Due to the lack of the detailed data about the Hall−Petch equation of the Mg−Ga alloys, k=220 MPa·μm$^{1/2}$ is adopted according to the references [14,15,17]. According to the study of SHI et al [15], it is also assumed that the value of k has nothing to do with the composition. The effect of solid solution strengthening can be expressed by [14,15,17]

$$\Delta\sigma_s=\sigma_{0.2}-\Delta\sigma_g=\sigma_{0.2}-(\sigma_0+kd^{-1/2}) \tag{4}$$

where $\sigma_{0.2}$ represents the yield strength, which can be obtained from Fig. 4, and $\Delta\sigma_g$ represents the contribution value of grain boundary strengthening. Solid solution strengthening $\Delta\sigma_s$ can be obtained by method mentioned above. Different solid solution models were developed [14,15,17] based on the solute concentration dependence of yield strength as follows:

$$\sigma_{ys}=\sigma_{y0}+Z_F G\xi_F^{3/2}c^{1/2} \tag{5}$$

$$\sigma_{ys}=\sigma_{y0}+Z_L G\xi_L^{4/3}c^{2/3} \tag{6}$$

where σ_{y0} is the yield stress of pure magnesium; Z_F and Z_L are constants, ξ_F and ξ_L are different linear combination of the size misfit parameter and the modulus misfit parameter, G is the shear modulus, and c is the molar fraction of solute atoms.

From the above two solid solution strengthening modes [14,15,17], it can be known that the solid solution strengthening effect of solute atoms is caused by the atomic size mismatch and the shear modulus mismatch. Therefore, these two equations should be generally applicable to describe the solid solution strengthening effect of different

alloying elements in magnesium alloys. The solid solution strengthening effect $\Delta\sigma_s$ of the Mg−Ga alloys is shown in Fig. 9. With the increase of Ga content, the $\Delta\sigma_s$ of alloy has a linear relationship with c^n. The slopes ($d\sigma/dc^n$) of the solid lines in Fig. 9 are 583 and 953 for n=1/2 and n=2/3, respectively. At the same time, the solid solution strengthening rates of other alloying elements are listed in Table 2, which are 118 and 196 (Al), 578 and 905 (Zn), 233 and 389 (Sn), 737 and 1429 (Y) and 683 and 1168 (Gd). Compared with the data in Table 2, the solid solution strengthening rate of Ga is higher than those of Al, Zn and Sn, and slightly lower than those of Y and Gd. According to Eqs. (5) and (6), both lattice parameters and shear modulus must be taken into account. The size difference between magnesium and the external atoms is an important factor directly, leading to the change of lattice parameters. Based on the Ref. [40], the sizes of different atoms and their differences with magnesium atoms are listed in Table 2. As displayed in Table 2, the size mismatch between Mg and Ga is larger than those between Mg and other alloy atoms. There is still a lack of reports on the elastic modulus of Ga. In the metal handbook, the elastic modulus of Ga is described as compressible at 20 °C [41], so it can be inferred that the elastic modulus of Ga is much smaller than Mg, Zn, Al, Sn, Y and Gd. The huge difference in elastic modulus is the reason that Ga has a good strengthening effect.

Based on the above analysis, the reason for the good solid solution strengthening effect of Ga

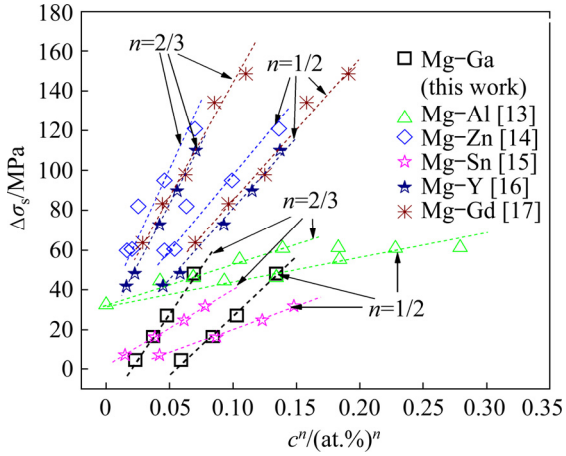

Fig. 9 Solid solution strengthening effect $\Delta\sigma_s$ of Mg−Ga alloys with Mg−Al, Mg−Zn, Mg−Sn, Mg−Y and Mg−Gd alloys for comparison (Data points of Fig. 4 re-plotted as function of c^n, after correcting for grain size effects using Eq. (3))

Table 2 Radius, atom size misfit δ, and strengthening rate (dHV/dc and $d\sigma/dc^n$) for Al, Zn, Sn, Y, Gd and Ga atoms in Mg alloy

Element	Radius/Å	δ	dHV/dc	$d\sigma/dc^{1/2}$	$d\sigma/dc^{2/3}$
Mg	1.601	–	–	–	–
Al	1.432	−10.6	3	118	196
Zn	1.395	−12.9	9	578	905
Sn	1.620	2.2	6.6	233	389
Y	1.802	12.6	13.23	737	1429
Gd	1.801	12.5	14	683	1168
Ga	1.392	−13.1	10.35	583	953

atoms in magnesium alloys can be summarized as follows: the mismatch of atomic size and modulus between Ga atoms and Mg atoms may be the reason for its better strengthening effect. The lattice distortion caused by the atomic size mismatch can hinder the movement of dislocations. According to the solid solution strengthening modes [14,15,17], the large degree of the modulus mismatch is also the reason why the addition of Ga atoms has a good strengthening effect. The XRD results in Fig. 2(b) show that with the solid solution of Ga atoms in the α-Mg matrix, the diffraction peak of α-Mg shifts to a high angle. According to the Bragg equation,

$$\lambda=2d\sin\theta \tag{7}$$

where d is the distance between crystal planes, θ is the Bragg diffraction angle, and λ is the wavelength. The crystal plane spacing decreases after the Ga atoms are dissolved in the α-Mg matrix since the atomic radius of the Ga atom is small. When the Ga atom dissolves in the α-Mg lattice, the lattice constant and the atomic spacing decrease, which increases the atomic binding force of Mg crystal and finally strengthens magnesium alloy [42]. The strengthening effects of Gd and Y elements cannot be explained by the classical theory, and the possible reasons for this phenomenon have also been analyzed in other studies [16,17].

4.2 Damping capacity

According to the Refs. [28,29], the damping of magnesium alloy at room temperature is caused by the bowing out motion of dislocation. The classical Granato-Lücke dislocation pinning model can be used to explain the damping properties of magnesium alloys. The total damping capacity (Q^{-1}) includes the strain-independent or weakly

dependent damping capacity (Q_0^{-1}) and strain-dependent damping capacity (Q_h^{-1}). The relationship of them can be expressed by

$$Q^{-1} = Q_0^{-1} + Q_h^{-1}(\varepsilon) \tag{8}$$

$$Q_0^{-1} = \frac{\rho B L_c^4 \omega}{36Gb^2} \tag{9}$$

$$Q_h^{-1} = (C_1/\pi\varepsilon)\exp(-C_2/\varepsilon) \tag{10}$$

where C_1, C_2 and B are constants; ρ is the movable dislocation density, excluding seriously entangled dislocations; b is the magnitude of Burger's vector of dislocations; ω is the angular frequency, which can be obtained from the experimental conditions; L_c is the distance between adjacent weak pinning points, which is the distance between solute atoms in the current study; C_1 and C_2 can be represented by

$$C_1 = \rho F_B L_N^3/(6bEL_c^2) \tag{11}$$

$$C_2 = F_B/(bEL_c) \tag{12}$$

$$C_1/C_2^2 = \rho bEL_N^3/(6F_B) \tag{13}$$

where L_N is the distance between adjacent strong pinning points on the dislocation. Only the grain boundary can be deemed as the strong pinning point in the current study since only a single-phase solid solution is concerned. The grain size can be considered as the distance between the adjacent strong pinning points (L_N). F_B is the force between point defects and dislocations, and E is the elastic modulus. When the strain amplitude is greater than the critical strain (ε_{cr1}) of dislocation removing from the weak pinning point, the relationship of Q_h^{-1} and C_1 and C_2 can be expressed as

$$\ln\left(\pi Q_h^{-1}\varepsilon\right) = \ln C_1 - C_2/\varepsilon \tag{14}$$

If the G−L curve ($\ln(\pi Q_h^{-1}\varepsilon)$ vs $1/\varepsilon$) is a straight line, then its damping behavior can be explained by the Granato−Lücke dislocation damping model. The G−L curves of Mg−Ga alloys are shown in Fig. 10. The linear fitting relationship between $\ln(\pi Q_h^{-1}\varepsilon)$ and $1/\varepsilon$ is satisfied until the strain amplitude reaches another critical value (ε_{cr2}). When the strain amplitude is higher than ε_{cr2}, the micro-plastic deformation occurs, and the damping mechanism of the alloys is changed into the micro-plastic damping mechanism [26]. The irreversible increment and the motion of dislocations in the micro-plastic damping mechanism are not described too much in this work. It can be found from Fig. 10 that the points under ε_{cr2} have a perfect linear distribution, which indicates that the damping properties of the Mg−Ga alloys can be explained well by the Granato−Lücke dislocation theory.

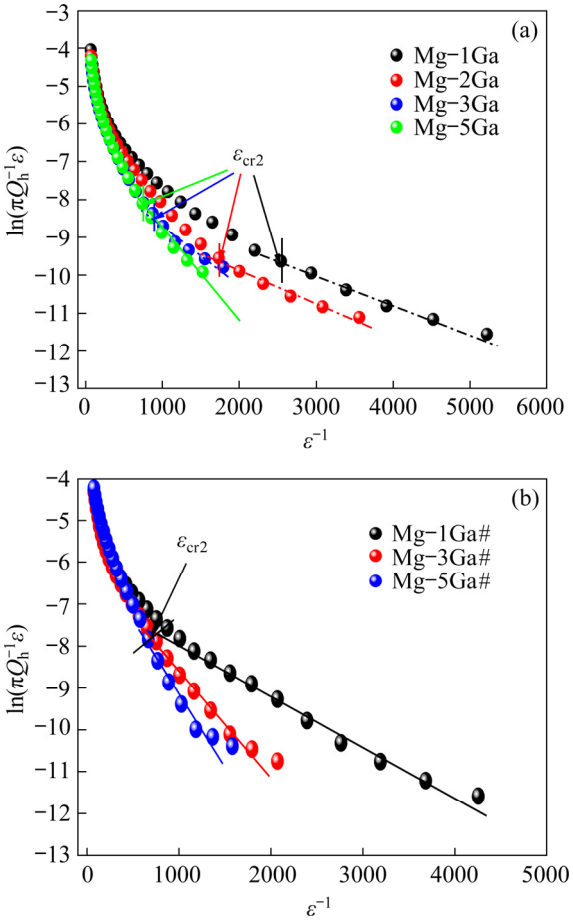

Fig. 10 G−L curves of solid solution treated Mg−Ga alloys: (a) Mg−Ga alloys; (b) Mg−Ga alloys with same grain size

It can be seen from Fig. 5 that the alloys with high Ga content have high damping properties at the low strain amplitude. Combined with Eq. (9), the existing theory holds that the damping capacity under the low strain amplitude is proportional to the quartic of the distance between the weak pinning points (L_c^4) [37,38]. The more the solute atoms are, the smaller the distance between the corresponding weak pinning points is, and the lower the damping capacity is, but the results of this study are contrary to it. The damping capacity of the alloy with higher Ga content is higher than that of the alloy with the lower Ga content. At the same time, this phenomenon has also been found in the other reports [43,44], but there is no corresponding analysis in these reports. Therefore, the strain-independent damping is not only related to L_c, but

also is affected by other factors. The previous research results showed that there was a great difference in the atomic radius and the modulus between Ga and Mg atoms, which makes the Ga element have better solid solution strengthening effect. The Ga atoms in solid solution treated Mg−Ga alloys existed in two ways [42]. Eight Mg atoms around Ga form a dodecahedral structure composed of the upper and lower hexahedrons, or two Ga solute atoms occupy the vertices of the upper and lower hexahedrons and combine with the seven Mg atoms sandwiched in the middle to form dodecahedral clusters. The schematic diagrams of two kinds of atomic configuration formed in the solution treated Mg−Ga are shown in Fig. 11(a). In addition, combined with the small radius of Ga atoms, the lattice distortion will be formed necessarily after the Ga atoms are dissolved in the α-Mg matrix. Therefore, just like the interaction between the dislocation and the GP region [30], the second phase [20,21] or stacking faults [31,32], the interaction between the dislocation and atomic configuration or lattice distortion will occur, thus improving the damping capacity. As a result, the Mg−Ga alloy has excellent damping properties.

It can be seen from Fig. 5(c) that with the increase of the Ga content to 5 wt.%, the damping capacity of the alloy decreases, which is related to the linear tension of dislocation. The linear tension of a dislocation is the force that straightens the bending dislocation. When the applied shear stress is balanced with it, the linear tension of dislocation (τ) can be expressed by

$$\tau = \frac{Gb}{2R} \tag{15}$$

where R is the radius of curvature of the dislocation. Under the low strain amplitude, the weak pinning point spacing L_c is equal to $2R$. Therefore, with the increase of the Ga content, the smaller the R is, the greater the linear tension of the dislocation is, which leads to the decrease of the mobility of the dislocation in the alloy with high Ga content and ultimately leads to the decrease of damping properties. Under the high strain amplitude, the alloy with a higher Ga content displays a lower damping capacity. This is due to the fact that the dislocation is separated from the weak pinning point and moves between the strong pinning points. Therefore, the alloy with a low Ga content, showing a large grain size, has a low line tension of dislocation, which leads to the increase of the mobility of the dislocation in the alloy with low Ga content and ultimately results in the increase of damping properties. When the strain amplitude is greater than the first critical strain amplitude, the damping capacities of all the alloys increase sharply, but the increase rate of the alloy with the high Ga content is high. It can be seen from Fig. 5(a) when the strain amplitude reaches a certain level (circled by red in Fig. 5(a)), the Mg−5Ga alloy exhibits higher damping capacity than the Mg−3Ga alloy. This phenomenon is even more pronounced in the alloy with the same grain size, which is illustrated in Fig. 6. This is due to the swinging between the strong pinning points when the dislocation is

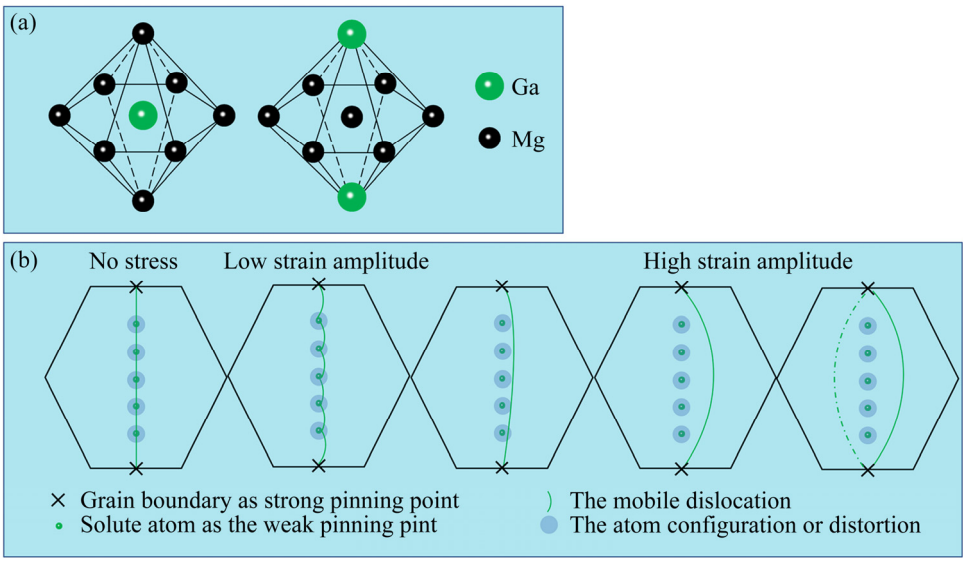

Fig. 11 Existent form of Ga atoms in α-Mg [42] (a), and improved G−L model (b)

unnailed, which will undoubtedly be affected by the atomic configuration and distortion formed by the solute atoms, just like the dislocation interact with the GP region [30], the second phase [20,21] or stacking faults [31,32]. As a result, the damping capacity of the alloy with a high Ga content increases rapidly.

Figure 10 shows that the damping properties of Mg−Ga alloys can be explained by the dislocation pinning model. It can be seen from the data in Table 3, the values of C_1 and C_2 increase with the increase of Ga content, while the value of C_1/C_2^2 decreases monotonously. From Eq. (13), the value of C_1/C_2^2 is related to L_N and F_B.

Table 3 Damping property parameters of solid solution treated Mg−Ga alloys

Alloy	$C_1/10^4$	$C_2/10^4$	$(C_1/C_2^2)/10^4$
Mg−1Ga	3.35	6.94	6.96
Mg−2Ga	2.23	7.74	3.72
Mg−3Ga	5.58	13.20	3.20
Mg−5Ga	12.07	21.50	2.61
Mg−1Ga#	11.45	12	7.95
Mg−3Ga#	21.63	24	3.76
Mg−5Ga#	39.80	34	3.44

After heat treatment, the grain boundaries acted as strong pinning point in Mg−1Ga#, Mg−3Ga# and Mg−5Ga# have little difference, the C_1/C_2^2 values of these alloys decrease continuously. Thus, it can be inferred that the increase of F_B value plays an obvious role and makes the C_1/C_2^2 value decrease. On the basis of the classical Granato−Lücke model [28,29], the influence of atomic configuration or lattice distortion is considered, and the schematic diagram of the improved model is shown in Fig. 11(b). From this model, it can be known that once the dislocation starts to move, it will interact with the atomic configuration or lattice distortion to achieve the internal friction, leading to the enhancement of the damping capacity.

The motion of dislocations is a thermal activation process, and the higher the temperature is, the stronger the kinetic energy of dislocations is. Therefore, the energy of dislocations is lower and the dislocations are not easy to move at room temperature. The results of Fig. 7 can further verify the model in Fig. 11(b). From Fig. 7, it can be seen that the damping capacity of Mg−5Ga is the best in the whole test temperature range, which is due to the large number of the unique atomic configuration or lattice distortion in Mg−5Ga. The higher the temperature is, the greater the probability of the dislocation interacting with such atomic configuration is, so that the damping capacity of the alloy with a high Ga content is greater. This further verifies that the Ga atoms are beneficial to the damping capacity improvement of the alloys.

5 Conclusions

(1) The relationship between the hardness of the Mg−Ga alloy and the Ga content can be expressed by the equation: $HV_{0.5}=41.61+10.35c$, where c is the molar fraction of solute atoms.

(2) With the increase in Ga content, the solid solution strengthening effect $\Delta\sigma_s$ of the alloy has a linear relationship with c^n. The solid solution strengthening effect of Ga is higher than these of Al, Zn and Sn due to the large atomic radius difference and the modulus mismatch between Ga and Mg atoms.

(3) The Mg−Ga alloys have excellent damping capacity and their damping value reaches a high damping level before the strain amplitude is less than the first critical strain amplitude, which is of great significance for the practical applications.

(4) The lattice distortion and the modulus mismatch generated because of the addition of Ga increase the resistance to motion of the dislocation when it is in the process of swinging or moving, thus the better damping capacity is acquired.

Acknowledgments

This work was supported by the National Natural Science Foundation of China (Nos. 51571089, 51871093), and the Natural Science Foundation of Hunan Province, China (No. 2019JJ40044).

References

[1] FENG Yan, WANG Ri-chu, PENG Chao-qun. Influence of freezing rate on microstructure and electrochemical properties of Mg−2%Ga alloys [J]. Transactions of Nonferrous Metals Society of China, 2011, 21(5): 1047−1051.

[2] FENG Yan, WANG Rr-chu, YU Kun, PENG Chao-qun, LI Wen-xian. Influence of Ga and Hg on microstructure and electrochemical corrosion behavior of Mg alloy anode

materials [J]. Transactions of Nonferrous Metals Society of China, 2007, 17(6): 1363−1366.

[3] KUBÁSEK J, VOJTĚCH D, LIPOV J, RUML T. Structure, mechanical properties, corrosion behavior and cytotoxicity of biodegradable Mg-X (X=Sn, Ga, In) alloys [J]. Materials Science and Engineering: C, 2013, 33: 2421−2432.

[4] KUBÁSEK J, VOJTĚCH D, DVORSKÝ D. Structural and mechanical study on Mg−*x*LM (*x*=0−5 wt.%, LM=Sn, Ga) alloys [J]. International Journal of Materials Research, 2016, 107(5): 459−471.

[5] MOHEDANO M, BLAWERT C, YASAKAU K A, ARRABAL R, MATYKINA E, MINGO B, SCHARNAGL N, FERREIRA M G S, ZHELUDKEVICH M L. Characterization and corrosion behavior of binary Mg−Ga alloys [J]. Materials Characterization, 2017, 128: 85−99.

[6] GAO Zhi-han, SONG Ming-shi, LIU Rui-liang, SHEN Yong-shuai, WARD L, COLE I, CHEN Xiao-bo, LIU Xin-chun. Improving in vitro and in vivo antibacterial functionality of Mg alloys through micro-alloying with Sr and Ga [J]. Materials Science and Engineering: C, 2019, 104: 109926.

[7] LIU Hong-bin, QI Guo-hong, MA Yu-tao, HAO Hai, JIA Fei, JI Shou-hua, ZHANG Huai-yue, ZHANG Xin-guo. Microstructure and mechanical property of Mg−2.0Ga alloys, Materials Science and Engineering: A, 2009, 526: 7−10.

[8] KHOKHLOVA J A, KHOKHLOV M A. 3d-visualization of magnesium strengthening mechanisms for a description of experimentally obtained data of alloying effect in Mg−Ga system [J]. Journal of Magnesium and Alloys, 2020, 8: 546−551.

[9] WU Dai-feng, OUYANG Liu-zhang, WU Cong, WANG Hui, LIU Jiang-wen, SUN Li-xian, ZHU Min. Phase transition and hydrogen storage properties of Mg−Ga alloy [J]. Journal of Alloys and Compounds, 2015, 642: 180−184.

[10] HUANG Wen-sen, CHEN Ji-hua, YAN Hong-ge, XIA Wei-jun, SU Bin, ZHU Wei-jun. Effects of Ga Content on dynamic recrystallization and mechanical properties of high strain rate rolled Mg−Ga alloys [J]. Metals and Materials International, 2020, 26: 747−759.

[11] HUANG Wen-sen, CHEN Ji-hua, YAN Hong-ge, XIA Wei-jun, SU Bin, YIN Hui, YAN Xiu-xiu. Microstructure, texture modification and mechanical anisotropy of high strain rate rolled Mg−Ga alloy sheets [J]. Journal of Materials Science，2020, 55: 10242−10257.

[12] OKAMOTO H. Ga−Mg (Gallium−Magnesium) [J]. Journal of Phase Equilibria & Diffusion, 2013, 34(2): 148.

[13] CÁCERES C H, ROVERA D M. Solid solution strengthening in concentrated Mg−Al alloys [J]. Journal of Light Metals, 2001, 1: 151−156.

[14] CÁCERES C H, BLAKE A. The strength of concentrated Mg−Zn solid solutions [J]. Physica Status Solidi (a), 2002, 194: 147−158.

[15] SHI Bing-qing, CHEN Rong-shi, KE Wei. Solid solution strengthening in polycrystals of Mg−Sn binary alloys. Journal of Alloys and Compounds, 2011, 509: 3357−3362.

[16] GAO Lei, CHEN Rong-shi, HAN En-hou. Solid solution strengthening behaviors in binary Mg−Y single phase alloys [J]. Journal of Alloys and Compounds, 2009, 472: 234−240.

[17] GAO Lei, CHEN Rong-shi, HAN En-hou. Effects of rare-earth elements Gd and Y on the solid solution strengthening of Mg alloys [J]. Journal of Alloys and Compounds, 2009, 481: 379−384.

[18] LUKÁČ P. Solid solution hardening in Mg−Cd single crystals [J]. Physica Status Solidi (a), 1992, 131: 377−390.

[19] SUGIMOTO K, NIIYA K, OKAMOTO T, KISHITAKE K. A study of damping capacity in magnesium alloys [J]. Transactions of the Japan Institute of Metals, 1977, 18: 277−288.

[20] WU Zhong-shan, WANG Jing-feng, WANG Hai-bo, MA She, HUANG Song, LI Shun, PAN Fu-sheng. Enhanced damping capacities of Mg−Ce alloy by the special microstructure with parallel second phase [J]. Journal of Materials Science & Technology, 2017, 33: 941−946.

[21] ZHANG J M, PEREZ R J, WONG C R, LAVERNIA E J. Effects of secondary phases on the damping behaviour of metals, alloys and metal matrix composites [J]. Materials Science and Engineering: R, 1994, 13: 325−389.

[22] WAN Di-qing, WANG Jing-cheng, WANG Gai-fang, LIN Lin, FENG Zhi-gang, YANG Gen-cang. Effect of eutectic phase on damping and mechanical properties of as-cast Mg−Ni hypoeutectic alloys [J]. Transactions of Nonferrous Metals Society of China, 2009, 19(1): 45−49.

[23] WANG Jing-feng, XU Dan-dan, LU Ruo-peng, PAN Fu-sheng. Damping properties of as-cast Mg−*x*Li−1Al alloys with different phase composition [J]. Transactions of Nonferrous Metals Society of China, 2014, 24(2): 334−338.

[24] YU Lang, YAN Hong-ge, CHEN Ji-hua, XIA Wei-jun, SU Bin, SONG Min. Effects of solid solution elements on damping capacities of binary magnesium alloys [J]. Materials Science and Engineering: A, 2020, 772: 138707.

[25] WAN Di-qing, HU Ying-lin, YE Shu-ting, LI Zhu-min, LI Li-li, HUANG Yi. Effect of alloying elements on magnesium alloy damping capacities at room temperature [J]. International Journal of Minerals, Metallurgy, and Materials, 2019, 26: 760−765.

[26] FAN Guo-dong, ZHENG Ming-yi, HU Xiao-shi, WU Kun, GAN Wei-min, BROKMEIER H G. Internal friction and microplastic deformation behavior of pure magnesium processed by equal channel angular pressing [J]. Materials Science and Engineering: A, 2013, 561: 100−108.

[27] HU Xiao-shi, HE Xiao-dong, ZHENG Ming-yi, WU Kun. Effect of small tensile deformation on damping capacities of Mg−1%Al alloy [J]. Transactions of Nonferrous Metals Society of China, 2010, 20: s444−s447.

[28] GRANATO A, LÜCKE K. Application of dislocation theory to internal friction phenomena at high frequencies [J]. Journal of Applied Physics, 1956, 27: 789−805.

[29] GRANATO A, LÜCKE K. Theory of mechanical damping due to dislocations [J]. Journal of Applied Physics, 1956, 27: 583−593.

[30] ZHOU Xiong-peng, YAN Hong-ge, CHEN Ji-hua, XIA Wei-jun, SU Bin, YU Lang, HUANG Wen-sen, SONG Min. Effects of low temperature aging precipitates on damping and mechanical properties of ZK60 magnesium alloy [J]. Journal of Alloys and Compounds, 2020, 819: 152961.

[31] XU Chi, ZHANG Jing-huai, LIU Shu-juan, JING Yong-bin, JIAO Yu-feng, XU Long-jiang, ZHANG Li, JIANG

Feng-chun, ZHANG Mi-lin, WU Rui-zhi. Microstructure, mechanical and damping properties of Mg−Er−Gd−Zn alloy reinforced with stacking faults [J]. Materials & Design, 2015, 79: 53−59.

[32] LI Zhen-zhen, YAN Hong-ge, CHEN Ji-hua, XIA Wei-jun, SU Bin, ZHAO Lu, SONG Min. Effect of Mg content on the damping behavior of Al−Mg alloys [J]. Metals and Materials International, 2021, 27: 3155−3163.

[33] PŮSKÁR A. Internal friction of metallic materials [M]. Berlin, Heidelberg: Springer, 2007.

[34] NIU Rui-long, YAN Fang-jia, WANG Yun-si, DUAN Dong-ping, YANG Xue-min. Effect of Zr content on damping property of Mg−Zr binary alloys [J]. Materials Science and Engineering: A, 2018, 718: 418−426.

[35] WAN Di-qing, WANG Jin-cheng, YANG Gen-cang. A study of the effect of Y on the mechanical properties, damping properties of high damping Mg−0.6%Zr based alloys [J]. Materials Science and Engineering: A, 2009, 517: 114−117.

[36] BLANTER M S, GOLOVIN I S, NEUH Ä USER H, SINNING H R. Internal friction in metallic materials [M]. Berlin: Springer, 2007.

[37] WANG Jing-feng, SONG Peng-fei, GAO Shan, HUANG Xue-fei, SHI Zhang-zhi, PAN Fu-sheng. Effects of Zn on the microstructure, mechanical properties, and damping capacity of Mg−Zn−Y−Zr alloys [J]. Materials Science and Engineering A, 2011, 528: 5914−5920.

[38] RIEHEMANN W, EL-AL F A. Influence of ageing on the internal friction of magnesium [J]. Journal of Alloys and Compounds, 2000, 310: 127−130.

[39] STARINK M J, WANG Shun-cai. A model for the yield strength of overaged Al−Zn−Mg−Cu alloys [J]. Acta Materialia, 2003, 51: 5131−5150.

[40] YE Y F, LIU X D, WANG S, LIU C T, YANG Y. The general effect of atomic size misfit on glass formation in conventional and high-entropy alloys [J]. Intermetallics, 2016, 78: 30−41.

[41] COMMITTEE A. Properties and selection: Nonferrous alloys and special-purpose materials [M]. 1990.

[42] LIU Hong-bin. Improving the strength / toughness of the magnesium alloys by alloying [D]. Dalian: Dalian University of Technology, 2009. (in Chinese)

[43] YUAN Jia-wei, LI Ting, ZHANG Kui, LI Meng, LI Xing-gang, LI Yong-jun, MA Ming-long, SHI Guo-liang. Effect of Zn content on the microstructures, mechanical properties, and damping capacities of Mg−7Gd−3Y−1Nd−0.5Zr based alloys [J]. Journal of Alloys and Compounds, 2019, 773: 919−926.

[44] WANG Jing-feng, LU Ruo-peng, WEI Wen-wen, HUANG Xue-fei, PAN Fu-sheng. Effect of long period stacking ordered (LPSO) structure on the damping capacities of Mg−Cu−Mn−Zn−Y alloys [J]. Journal of Alloys and Compounds, 2012, 537: 1−5.

Mg−Ga 二元合金的固溶强化和阻尼性能

黄文森[1,2]，陈吉华[1,2]，严红革[1,2]，李 强[3]，夏伟军[1,2]，苏 斌[1,2]，朱伟俊[1]

1. 湖南大学 材料科学与工程学院，长沙 410082；
2. 湖南大学 湖南省喷射沉积技术与应用重点实验室，长沙 410082；
3. 北京航天长征飞行器研究所，北京 100076

摘 要：利用光学显微镜(OM)、扫描电子显微镜(SEM)、X 射线衍射(XRD)、硬度测试、拉伸测试和动态机械分析仪(DMA)研究 Ca 含量为 1%~5%(质量分数)的 Mg−Ga 二元合金的力学性能和阻尼性能。研究发现，合金的硬度($HV_{0.5}$)随着 Ga 含量的增加而增加，硬度与 Ga 含量的关系为: $HV_{0.5}=41.61+10.35c$，Mg−Ga 合金的固溶强化贡献值 $\Delta\sigma_s$ 与 c^n 呈线性关系，其中 c 为溶质原子浓度，n=1/2 或 2/3。Ga 和 Mg 原子之间的较大原子半径差异和模量差异使得 Ga 表现出比 Al、Zn 和 Sn 更强的固溶强化效果。Ga 的添加使得 Mg−Ga 合金具有很好的阻尼性能，这种现象可以通过 Granato−Lücke 位错模型来解释。Ga 添加形成的晶格畸变和模量失配增加位错在摆动和运动过程中所受到的阻力，从而获得很好的阻尼性能。

关键词：Mg−Ga 合金；固溶强化；阻尼性能；Granato−Lücke 模型

(Edited by Xiang-qun LI)